

Colloidal transport through optical tweezer arrays

Yael Roichman,¹ Victor Wong,² and David G. Grier¹

¹*Department of Physics and Center for Soft Matter Research, New York University, New York, NY 10003*

²*Stuyvesant High School, New York, NY 10282*

(Dated: February 8, 2020)

Viscously damped particles driven past an evenly spaced array of potential energy wells or barriers may become kinetically locked in to the array, or else may escape from the array. The transition between locked-in and free-running states has been predicted to depend sensitively on the ratio between the particles' size and the separation between wells. This prediction is confirmed by measurements on monodisperse colloidal spheres driven through arrays of holographic optical traps.

Particles rolling down a sinusoidally modulated slope constitute an archetype for problems as diverse as the electrodiffusion of atoms on crystals, the transport characteristics of Josephson junctions and the entire field of chemical kinetics. The one-dimensional tilted washboard problem has been studied exhaustively. Considerably less is known for related problems in higher dimensions. Recently, attention has become focused on the transport of viscously damped colloidal particles flowing through two-dimensional potential energy landscapes. This system can be realized in practice by passing fluid-borne objects through microfabricated arrays of posts [1, 2, 3, 4], over arrays of electrodes [5, 6] and through periodically structured light fields [7, 8, 9].

Experimental realizations of two-dimensionally modulated transport are interesting both because they provide

insights into the underlying fundamental problem, and also because they constitute an entirely new category of sorting techniques. Different types of objects, it turns out, can follow dramatically different paths through the same physical landscape. Sorting fluid-borne objects by size, shape and composition have been demonstrated in this way [8, 9]. Preliminary theoretical studies [9, 10] suggest that periodic landscapes can act as extraordinarily selective sieves, for example sorting spheres by size with exponential resolution. This article presents experimental confirmation of some of these theories' predictions.

Our system, shown schematically in Fig. 1, tracks the motions of monodisperse colloidal spheres as they are driven back and forth over static potential energy landscapes created with arrays of holographic optical traps. The samples consist of colloidal silica spheres $a = 0.75 \pm 0.075 \mu\text{m}$ in radius (Bangs Laboratories 5303) These spheres were dispersed in deionized water and hermetically sealed in a slit pore formed by bonding the edges of a #1 cover slip to the face of a glass microscope slide. The glass surfaces were treated by oxygen plasma etching before assembly to increase their surface charge and thereby prevent particle deposition. The sample was rigidly mounted on a Prior Proscan II translation stage integrated into a Nikon TE2000U optical microscope, where it was allowed to equilibrate to room temperature, $T = 296 \pm 2 \text{ K}$.

Previous experimental studies of transport through static light fields have driven the spheres electrokinetically, optophoretically [11] or hydrodynamically [7, 8, 9]. Others have swept the light field through stationary samples [12, 13, 14, 15, 16, 17]. We instead used the motorized stage to translate the entire sample past stationary patterns of optical traps. All particles consequently traveled past the traps at the same velocity, \mathbf{v} , without complications due to nonuniform flow profiles [9] and without time-dependent ratchet phenomena [14]. Roughly 5,000 particles were repeatedly passed back and forth over the same field of view at constant speed and a variety of angles to build up a statistically well sampled set of data for each set of conditions. Repeatedly revisiting the same part of the sample cell with the same particles minimized effects due to nonuniform sample thickness and variability in the spheres' properties.

Images of the moving particles were recorded as an un-

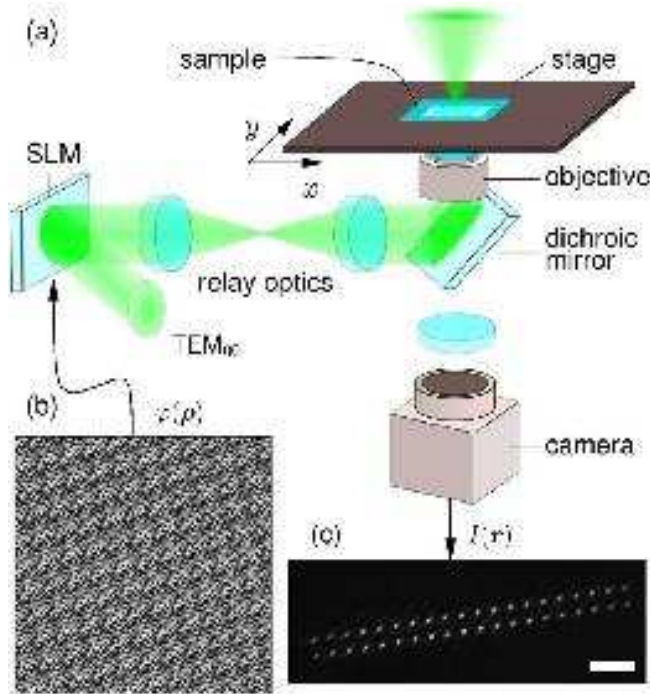


FIG. 1: Colloidal transport through an array of holographic optical traps. (a) Holographic trapping system. (b) Phase hologram $\varphi(\boldsymbol{\rho})$ encoding a 20×2 array of optical traps, shown in (c). Scale bar indicates $5 \mu\text{m}$.

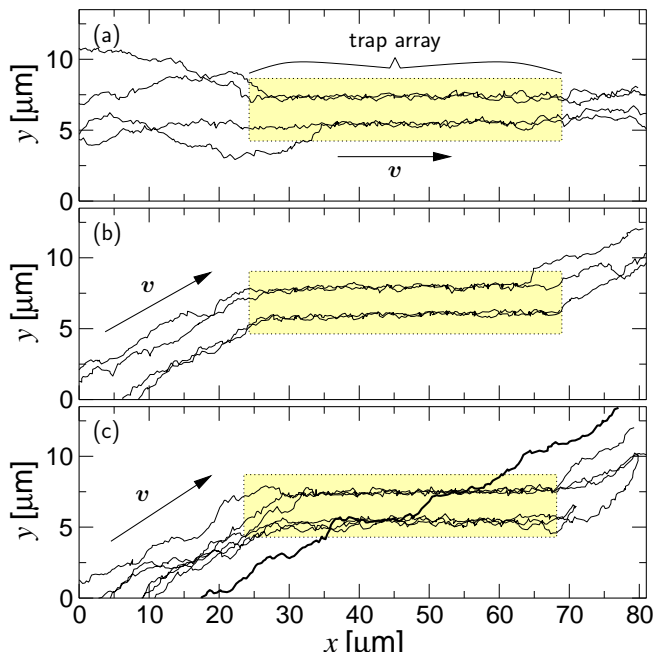


FIG. 2: Selected trajectories of $a = 0.75 \mu\text{m}$ diameter silica spheres flowing at $v = 10 \mu\text{m/s}$ through an array of optical traps with $b = 2.025 \mu\text{m}$ at $P = 0.85 \text{ W}$. The shaded boxes indicate the extent of the optical trap array. (a) Aligned: $\theta = 0^\circ$. (b) Kinetically locked in at $\theta = 10^\circ$. (c) Marginally locked in at $\theta_m = 12^\circ$. For $\theta \geq \theta_m$, some particles escape the array.

compressed digital video stream using an NEC TI-324A video camera and a Pioneer 520HS digital video recorder. The combination of a $100\times$ oil immersion objective lens (Nikon Plan Apo, NA 1.4) and a $0.63\times$ video eyepiece provides a field of view of $86 \times 63 \mu\text{m}^2$ and a magnification of $0.135 \mu\text{m}$ per pixel. Spheres' images were subsequently digitized into trajectories with 20 nm spatial resolution at $1/30 \text{ s}$ intervals using standard methods of digital video microscopy [18]. Typical measured trajectories are plotted in Fig. 2.

The moving spheres encountered point-like optical tweezers [19] projected in a 20×2 grid with the holographic optical trapping technique [20, 21, 22]. All of the traps were created from a single beam of laser light at wavelength $\lambda = 532 \text{ nm}$ and power $P = 0.85 \text{ W}$ provided by a frequency-doubled diode pumped solid state laser (Coherent Verdi). This beam was diffracted into an array of trap-forming beams by a phase-only computer-generated hologram, $\varphi(\rho)$, an example of which appears in Fig. 1(b). The diffracted beams then were relayed to the objective lens, which focused them into traps. Imprinting the hologram on the beam's wavefronts with a computer-addressed spatial light modulator (SLM, Hamamatsu X7269 PPM) allows for sequences of trapping patterns to be projected with different lattice constants and orientations. Laser light is reflected into the objective lens with a tuned dichroic mirror (Chroma Technologies) with a reflectivity of 99.5 per-

cent at $\lambda = 532 \text{ nm}$. This mirror transmits light at other wavelengths, which therefore can be used to create images of the spheres.

The image of the focused traps in Fig. 1(c) was obtained by placing a front surface mirror in the lens' focal plane. Enough of the reflected laser light passes through the dichroic mirror to create a clear low-noise image of the trapping pattern. Images such as this were used to adaptively improve the traps' uniformity [22]. After iterative improvement, the traps' intensities typically varied by less than 15 percent from the mean.

Each colloidal particle experiences an optical trap as radially symmetric potential energy well whose depth, $V_0(a)$, and width, $\sigma(a)$, both depend on the particle's shape, size and composition [10]. The trap's depth also is proportional to the total laser power, P . If a particle is deflected enough by its encounter with one trap to fall into another trap's domain of influence, it can become kinetically locked in to a commensurate trajectory through the array of traps [7, 9, 10, 23]. If, on the other hand, the driving force is too strong, or the required deflection angle too steep, the particle escapes from the traps and runs freely downstream. In our experiment, the driving force, $\mathbf{F}_0(a) = \gamma(a) \mathbf{v}$, is the hydrodynamic drag on a sphere of radius a driven through a quiescent fluid at velocity \mathbf{v} . The viscous drag coefficient, $\gamma(a)$, is proportional to the fluid's viscosity and accounts for hydrodynamic coupling to the bounding walls [24, 25, 26, 27].

The data in Fig. 2 were obtained at $v = 10 \mu\text{m/s}$ so that each sphere crossed the entire field of view within $t = 9 \text{ s}$. By contrast, the spheres' measured [18, 22] self-diffusion coefficient, $D = 0.10 \pm 0.01 \mu\text{m}^2/\text{s}$, corresponds to a thermally driven displacement of just $\sqrt{2Dt} = 0.6 \mu\text{m}$ in the same period. The associated viscous drag coefficient, $\gamma = k_B T/D = 40 \text{ fN s}/\mu\text{m}$ suggests that the spheres were driven past the traps with a maximum force of roughly $F_0 = 0.4 \text{ pN}$.

The distinction between locked-in and free trajectories becomes clear when the driving force \mathbf{F}_0 is inclined with respect to the array, as shown in Fig. 2(b). In this case, the locked-in trajectories are deflected by angle θ with respect to \mathbf{F}_0 . This deflection is the basis for continuous sorting techniques in which different fractions of a mixed sample are deflected to different angles by the same optical intensity field [7, 8, 9].

All trajectories become locked in when the driving force is aligned with the traps, $\theta = 0^\circ$; they all escape for $\theta = 90^\circ$. The maximum angle, θ_m , to which a spherical object can be deflected by a periodic optical intensity field before it escapes has been predicted to depend exceptionally strongly on the object's radius [9, 10, 28]. This is a purely kinematic effect, and not the result of thermal activation over potential energy barriers, as has been suggested [8].

Modeling the optical traps as Gaussian potential energy wells separated by distance b yields [9, 10]

$$\sin \theta_m = |S(a)| \exp\left(-\frac{b^2}{8\sigma^2(a)}\right), \quad (1)$$

with the prefactor,

$$S(a) = \frac{2}{\sqrt{e}} \frac{V_0(a)}{\sigma(a)F_0(a)}, \quad (2)$$

reflecting a balance between trapping and driving forces at the point of escape. The traps' effective width is given by

$$\sigma^2(a) = a^2 + \frac{\lambda^2}{4n^2}, \quad (3)$$

where n is the fluid's index of refraction. For the particles in our study, dispersed in water with $n = 1.33$, $\sigma = 0.85 \mu\text{m}$. Similar results are obtained for more general periodic landscapes [10], with Eq. (1) representing the leading term in a Fourier expansion of the trapping potential. Equation (1) also applies for arrays of barriers rather than wells [10].

According to Eq. (1), the marginally locked-in angle, θ_m , depends very strongly on the ratio $b/\sigma(a)$, and thus on particle size for $a > \lambda$. This is the basis for the assertion [9] that sorting by transport through a periodic landscape can offer exponential size selectivity. This prediction, however, results from limiting arguments that have not been tested experimentally. More rigorous results are available only in the limit that $V_0 \ll F_0\sigma \approx k_B T$, in which case thermal forces cannot be neglected and the escape transition is expected to be less dramatic [29].

We explicitly tested the predicted dependence on trap separation, b , and laser power by driving monodisperse particles past adaptively optimized trap arrays at fixed speed, v , over a range of angles, gauging the marginal angle by the suddenly increasing proportion of escaping trajectories. As θ approaches θ_m , particles' trajectories become increasingly sensitive to variations in the traps'

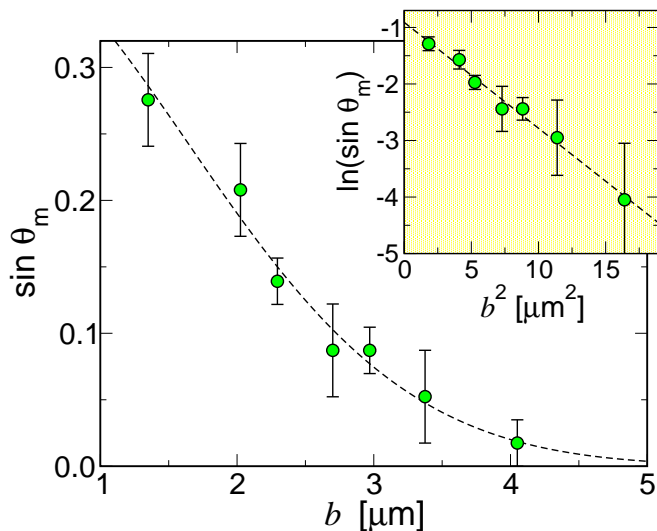


FIG. 3: Dependence of the marginally locked in angle as a function of lattice constant. Inset: The data replotted to emphasize the comparison to Eq. (1).

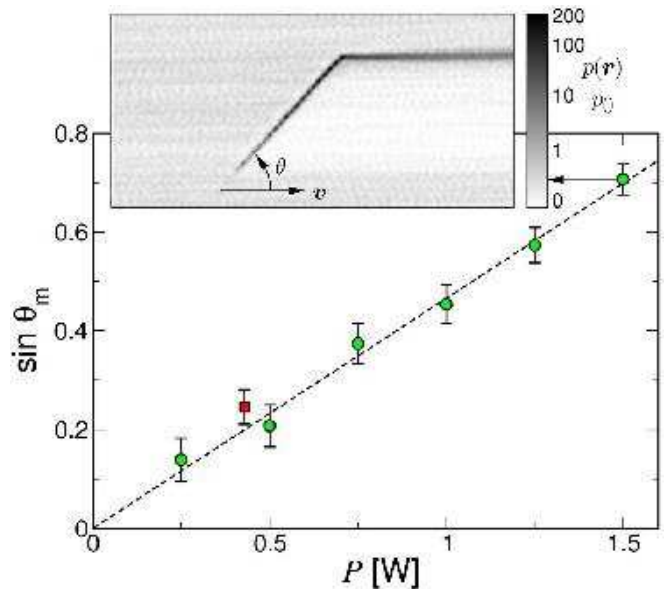


FIG. 4: Dependence of the marginally locked in angle on total projected laser power for fixed values of lattice constant, $b = 1.35 \mu\text{m}$, and speed, $v = 46 \mu\text{m/s}$. The square point is replotted from Fig. 3. Inset: Probability density $p(r)$ to find a particle at r , normalized by the bulk value, p_0 , at $\theta = 45^\circ$. The downstream shadow in $p(r)$ demonstrates effectively perfect large-angle deflection for $P = 1.5 \text{ W}$. Average over 500 trajectories.

intensities, to thermal fluctuations, and to small differences in individual particles' radii. A typical escape transition is apparent in the selected trajectories plotted in Fig. 2(c). It is reasonable to expect that the first observed escape events would involve the smallest particles interacting with the weakest traps. Analyzing particle tracks, however, did not provide sufficient size resolution to test this directly. The marginally locked-in angle for a particular choice of b was determined by analyzing roughly 2000 such trajectories for each value of θ ranging from 0° to 30° in 2° increments.

Results for $\theta_m(b)$, obtained at fixed speed, v , and laser power, P , are plotted in Fig. 3. The dashed curve is a one-parameter fit to Eq. (1), where only the overall scale, $S(a)$, is treated as a free parameter. The fit value, $S(a) = 0.40 \pm 0.01$ corresponds to a well depth of roughly $100 k_B T$, which is reasonable for traps powered with 2 mW of light. The experimental results' excellent agreement with the prediction suggests that Eq. (1) quantitatively describes colloidal transport through an array of optical traps.

The marginally locked-in angle can be tuned for maximum sensitivity by adjusting b . Its magnitude can be set independently through the prefactor, $S(a)$. In particular, $S(a)$ should scale linearly with laser power, P , through its dependence on V_0 . Thus θ_m for a given size of particle can be adjusted with laser power, for fixed v , up to the point that particles begin to get stuck in the traps. The data in Fig. 4 demonstrate that deflection angles as large

as $\theta_m = 45^\circ$ can be attained in this way. They therefore contradict the assertion [8] that arrays of discrete traps are incapable of deflecting trajectories over large angles.

The data in Fig. 4 were obtained with a single row of 20 traps at fixed inter-trap separation of $b = 1.35 \mu\text{m}$, and with particles driven at $v = 46 \mu\text{m/s}$. Using a single line of traps increases the possibility that particles might leak through the array, but doubles the accessible range of laser powers. Data from Fig. 3 at the same particle speed and lattice constant fall on the same curve once the laser power is rescaled. The observed linear dependence of $\sin \theta_m$ on laser power, P , confirms the predicted dependence on the prefactor, $S(a)$ in Eq. (1).

The plot inset into Fig. 4 provides an overview of the data obtained at $\theta_m = 45^\circ$ and $P = 1.5 \text{ W}$. It shows the probability distribution $p(\mathbf{r})$ for finding a particle within 200 nm of \mathbf{r} , integrated over 500 trajectories, comprising roughly 30,000 separate particle images. The probability distribution is normalized by the probability, p_0 , of finding a particle in the undeflected stream over the same period. Darker regions indicate a higher-than-average probability density and lighter regions indicate lower-than-average probabilities. Details in the distribution are emphasized with a nonlinear color table, which

also is inset. The results show that particles are strongly concentrated in the traps themselves and work their way up the array until they escape at its end. The nearly perfect deflection of the incident stream of particles leaves a sharply defined shadow in the probability density downstream of the traps. A total of 15 of the 500 particles escaped the array near its end, most likely representing the smallest end of the particle size distribution.

Confirming the marginally locked-in angle's dependence on trap separation and laser power supports the assumptions made in deriving Eq. (1), particularly because the predicted form for $\sigma(a)$ agrees quantitatively with experimental results. This provides additional, albeit indirect, support for the prediction that athermal sieving by periodically modulated landscapes can sort objects with exponential size selectivity. It leaves open questions regarding the nature of transitions among different commensurate locked-in states in more extensive two-dimensional lattices. It also does not address the nature of colloidal transport through aperiodic landscapes, such as quasiperiodic arrays of optical traps. Experiments to address these questions are in progress.

This work was supported by the National Science Foundation through Grant Number DMR-0451589.

-
- [1] R. H. Carlson, C. V. Gabel, S. S. Chan, and R. H. Austin, Phys. Rev. Lett. **79**, 2149 (1997).
 - [2] T. A. J. Duke and R. H. Austin, Phys. Rev. Lett. **80**, 1552 (1997).
 - [3] C.-F. Chou, O. Bakajin, S. W. P. Turner, T. A. J. Duke, S. S. Chan, E. C. Cox, H. G. Craighead, and R. H. Austin, Proc. Nat. Acad. Sci. **96**, 13762 (1999).
 - [4] C. F. Chou, R. H. Austin, O. Bakajin, J. O. Tegenfeldt, J. A. Castellino, S. S. Chan, E. C. Cox, H. Craighead, N. Darnton, T. Duke, et al., Electrophoresis **21**, 81 (2000).
 - [5] T. P. Hunt, H. Lee, and R. M. Westervelt, Appl. Phys. Lett. **85**, 6421 (2004).
 - [6] P. Y. Chiou, T. Ohta, Aaron, and M. C. Wu, Nature **436**, 370 (2005).
 - [7] P. T. Korda, M. B. Taylor, and D. G. Grier, Phys. Rev. Lett. **89**, 128301 (2002).
 - [8] M. P. MacDonald, G. C. Spalding, and K. Dholakia, Nature **426**, 421 (2003).
 - [9] K. Ladavac, K. Kasza, and D. G. Grier, Phys. Rev. E **70**, 010901(R) (2004).
 - [10] M. Pelton, K. Ladavac, and D. G. Grier, Phys. Rev. E **70**, 031108 (2004).
 - [11] S.-H. Lee and D. G. Grier, Phys. Rev. Lett. **96**, 190601 (2006).
 - [12] S.-H. Lee, K. Ladavac, M. Polin, and D. G. Grier, Phys. Rev. Lett. **94**, 110601 (2005).
 - [13] S.-H. Lee and D. G. Grier, Phys. Rev. E **71**, 060102(R) (2005).
 - [14] S.-H. Lee and D. G. Grier, J. Phys.: Condens. Matt. **17**, S3685 (2006).
 - [15] T. Čižmár, M. Šiler, M. Šerý, P. Zemánek, V. Garcés-Chávez, and K. Dholakia, Phys. Rev. B **74**, 035105 (2006).
 - [16] B. A. Koss and D. G. Grier, Appl. Phys. Lett. **82**, 3985 (2003).
 - [17] I. Ricárdez-Vargas, P. Rodríguez-Montero, R. Romo-García, and K. Volke-Supúlveda, Appl. Phys. Lett. **88**, 121116 (2006).
 - [18] J. C. Crocker and D. G. Grier, J. Colloid Interface Sci. **179**, 298 (1996).
 - [19] A. Ashkin, J. M. Dziedzic, J. E. Bjorkholm, and S. Chu, Opt. Lett. **11**, 288 (1986).
 - [20] E. R. Dufresne and D. G. Grier, Rev. Sci. Instr. **69**, 1974 (1998).
 - [21] J. E. Curtis, B. A. Koss, and D. G. Grier, Opt. Comm. **207**, 169 (2002).
 - [22] M. Polin, K. Ladavac, S.-H. Lee, Y. Roichman, and D. G. Grier, Opt. Express **13**, 5831 (2005).
 - [23] A. Gopinathan and D. G. Grier, Phys. Rev. Lett. **92**, 130602 (2004).
 - [24] J. Happel and H. Brenner, *Low Reynolds Number Hydrodynamics* (Kluwer, Dordrecht, 1991).
 - [25] C. Pozrikidis, *Boundary Integral and Singularity Methods for Linearized Viscous Flow* (Cambridge University Press, New York, 1992).
 - [26] E. R. Dufresne, T. M. Squires, M. P. Brenner, and D. G. Grier, Phys. Rev. Lett. **85**, 3317 (2000).
 - [27] E. R. Dufresne, D. Altman, and D. G. Grier, Europhys. Lett. **53**, 264 (2001).
 - [28] J. M. Sancho, M. Khoury, K. Lindenberg, and A. M. Lacasta, J. Phys.: Condens. Matt. **17**, S4151 (2005).
 - [29] J. P. Gleeson, J. M. Sancho, A. M. Lacasta, and K. Lindenberg, Phys. Rev. E **73**, 041102 (2006).